Magnetic structure of Tb_3NbO_7 determined using neutron diffraction experiments and magnetic anisotropy calculations

Masashi Hase[a], Andreas Dönni[a], Vladimir Yu. Pomjakushin[b], Martin Rotter[c]

[a] *Research Center for Materials Nanoarchitectonics (MANA), National Institute for Materials Science (NIMS), Tsukuba, 305-0047, Ibaraki, Japan*
[b] *Laboratory for Neutron Scattering and Imaging, Paul Scherrer Institute (PSI), Villigen PSI, CH-5232, Switzerland*
[c] *McPhase Project, Venice, 30121, Italy*

Abstract

We determined the magnetic structure of Tb_3NbO_7 based on powder neutron diffraction experiments and magnetic anisotropy calculations. We calculated the energy levels split by crystalline electric fields, and the magnetic moments using McPhase. The c axis is the easy axis for Tb1 moments, and magnetic anisotropy is small for Tb2 moments. Magnetic reflections were observed at low temperatures. The propagation vector is $\mathbf{k}_1 = (0, 0, 0)$ at 1.8 K and $\mathbf{k}_2 = (1/2, 1/2, 0)$ at 2.5 K between transition temperatures $T_{N1} = 2.0$ K and $T_{N2} = 3.2$ K. We selected candidates for an irreducible representation (IR) of the magnetic structures using magnetic anisotropy. From Rietveld refinements, we determined the following: The IRs are $m\Gamma_4$ and mS_2 at 1.8 K and 2.5 K, respectively. The main component of Tb1 ordered moments is w at 1.8 K. The order of the main components in each chain along the c axis is antiferromagnetic. Tb1 moments are disordered at 2.5 K. Tb2 moments form noncollinear magnetic structures in the ab plane perpendicular to Tb1 chains with a small w component at both the 1.8 K and 2.5 K. The magnetic structure at 1.8 K is consistent with the magnetic anisotropies obtained using McPhase calculations. Only Tb2 moments are ordered at 2.5 K, indicating the appearance of a partially disordered state. We also considered the origin of the two magnetic transitions.

Keywords:
Magnetic structures of Tb_3NbO_7, Magnetic anisotropy calculations using

McPhase, Two propagation vectors, Partially disordered state,

1. Introduction

Selection of the propagation vector and irreducible representation (IR) is important to determine magnetic structures using neutron diffraction datasets [1, 2]. However, it is difficult to select a correct IR among many candidates of IR. Therefore, we narrow down IRs considering the other results. For example, when we know the signs of exchange interactions or appearance of spontaneous magnetization, IRs consistent with the results remain as candidates.

Furthermore, magnetic anisotropy is crucial in selecting a correct IR. For example, when the c axis is the easy axis of the magnetic moments, IRs with finite c (w) components are candidates. The magnetic moments and anisotropy can be calculated using McPhase, which is an open source program package for the calculation of magnetic properties [3, 4, 5]. In addition, McPhase plays an important role in the analysis of magnetic structures [6, 7, 8, 9, 10]. Therefore, we focus on McPhase to efficiently determine magnetic structures.

We focus on Tb_3NbO_7 [11] because of the following two results. One result is the appearance of two magnetic transitions in R_3AO_7 (R = Tb or Nd, A = nonmagnetic ion) [17]. In R_3MO_7 (R = Tb or Nd, M = magnetic ion), on the other hand, one magnetic transition occurs. We confirmed that both R and Ru magnetic moments ordered at the same antiferromagnetic (AFM) transition temperature T_N = 17 K [14] and 19 K [16] in R_3RuO_7 (R = Tb and Nd), respectively, indicating existence of interactions between R and Ru magnetic moments [12]. Therefore, it is expected that the magnetic model is simpler in R_3AO_7 than in R_3MO_7, whereas mechanism of appearance of the magnetic order may be more complicated in R_3AO_7 because of the two magnetic transitions.

The other result is the unique magnetic structure of Tb_3RuO_7 as shown in Fig. 1(a) [12, 13]. Tb_3NbO_7 and Tb_3RuO_7 are nearly isostructural. There are six crystallographic Tb sites, and two crystallographic Ru sites in Tb_3RuO_7. The Tb1 (blue) and Tb2 (light-blue) ordered moments are parallel to the b axis along which Tb1-Tb2 chains are formed. The order of the Tb1 and Tb2 moments is AFM in each Tb1-Tb2 chain. The Tbi ($i = 3 - 6$) moments (red) form a noncollinear magnetic structure in the ac plane perpendicular

to Tb1-Tb2 chains. The Ru1 and Ru2 moments are ordered and disordered (paramagnetic), respectively, indicating the presence of a partially disordered state, although the two Ru sites are very similar. In the family of R_3RuO_7 (R = rare earth elements), magnetic structures of Tb_3RuO_7 and Nd_3RuO_7 have been determined [12]. They are significantly different from each other, although the two compounds are nearly isostructural [14, 15, 16, 17].

Here, we describe the magnetism and crystal structure of Tb_3NbO_7 [11]. The magnetic susceptibility and specific heat of a powder sample were measured. The first and second order phase transitions occurred at $T_{N1} = 2.0$ and $T_{N2} = 3.2$ K, respectively. It was speculated that Tb1 and Tb2 moments were ordered at $T_{N1} = 2.0$ and $T_{N2} = 3.2$ K, respectively [11]. No spontaneous magnetization appeared down to 1.8 K. The magnetic susceptibility shows a broad maximum at around 4 K, probably indicating existence of short-range magnetic correlations. Figure 1(b) shows the Tb positions. The space groups of Tb_3NbO_7 and Tb_3RuO_7 in the low-temperature (T) phase are orthorhombic $C222_1$ (No. 20) [11] and $Pna2_1$ (No. 33) [14], respectively. The a, b, and c axes in Tb_3NbO_7 correspond to the a, c, and b axes in Tb_3RuO_7, respectively. There are two crystallographic Tb sites. Tb1 (blue) and Tb2 (red) sites in Tb_3NbO_7 correspond to the Tbi ($i = 1 - 2$) and Tbi ($i = 3 - 6$) sites in Tb_3RuO_7, respectively. Thus, a Tb1 chain along the c axis in Tb_3NbO_7 corresponds to a Tb1-Tb2 chain along the b axis in Tb_3RuO_7. These two compounds are isostructural in the high-T phase [14, 19, 20]. The space group is orthorhombic $Cmcm$ (No. 63). Figure 1(c) shows oxygen ions around Tb ions. Oxygen ions form cubic-like square prism and pentagonal bipyramid around Tb1 and Tb2 ions, respectively.

It is necessary to determine the magnetic structure of Tb_3NbO_7 to investigate mechanism of appearance of the magnetic order and to understand the magnetic structure of Tb_3RuO_7. Consequently, we performed powder neutron diffraction experiments on the Tb_3NbO_7, determined the magnetic structure of Tb_3NbO_7 using supports of McPhase, and then compared with the magnetic structure of Tb_3RuO_7.

2. Methods of experiments and calculations

We synthesized crystalline powders of Tb_3NbO_7 via a solid-state reaction. The starting materials were Tb_4O_7 and Nb_2O_5 powders with purities of 99.99% and 99.9%, respectively. Stoichiometric mixtures of the powders were sintered at 1673 K for 24 h in air. Powder X-ray diffraction patterns

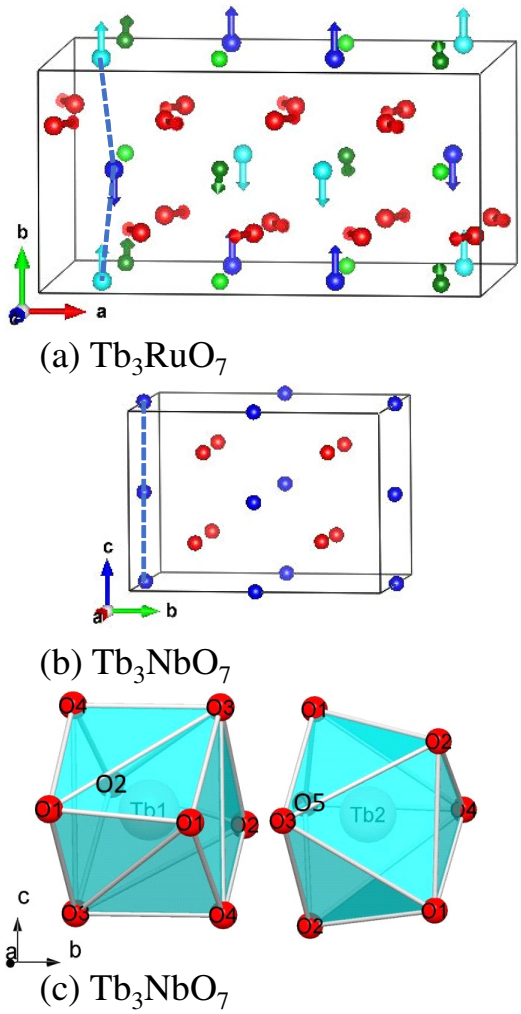

Figure 1: (a) Magnetic structure of Tb_3RuO_7 at 1.5 K [12] drawn using VESTA [18]. The space group of the low-T phase is orthorhombic $Pna2_1$ (No. 33) [14]. The lattice constants are $a = 14.588$ Å, $b = 7.345$ Å, and $c = 10.560$ Å at room temperature. The rectangular represents a unit cell. Blue, light-blue, red, green, and light-green circles denote Tb1, Tb2, Tbi ($i = 3-6$), Ru1, and Ru2 sites, respectively. Tb1-Tb2 chains indicated by the dashed line are formed along the b axis. (b) Tb positions in the low-T phase of Tb_3NbO_7. The space group is orthorhombic $C222_1$ (No. 20) [11]. The lattice constants are $a = 7.465$ Å, $b = 10.552$ Å, and $c = 7.514$ Å at room temperature. The rectangular represents a unit cell. The a, b, and c axes in Tb_3NbO_7 correspond to the a, c, and b axes in Tb_3RuO_7, respectively. The blue and red circles denote Tb1 and Tb2 sites, respectively. Tb1 chains indicated by the dashed line are formed along the c axis. (c) Oxygen ions around Tb ions in Tb_3NbO_7.

were recorded at room temperature using an X-ray diffractometer (RINT-TTR III, Rigaku). Within the experimental accuracy range the obtained sample was in a single phase.

Neutron diffraction experiments were performed at the Swiss Spallation Neutron Source of the Paul Scherrer Institut, where the high-resolution powder diffractometer for thermal neutrons (HRPT diffractometer) [21] was used. We performed group-theory analysis of magnetic structures using the programs ISODISTORT [1] and BasIreps in the FullProf Suite program package [2]. We performed Rietveld refinements of crystal and magnetic structures using the FullProf Suite program package [2] containing the internal tables for scattering lengths, and magnetic form factors. We calculated energy levels split by crystalline electric fields (CEFs) and magnetic moments using McPhase [3, 4, 5].

3. Results and discussion

3.1. Crystal structure at 12.0 K

The blue circles in Fig. 2 represent the neutron diffraction patterns of Tb_3NbO_7 at 12.0 K. We performed Rietveld refinements in the orthorhombic space group $C222_1$ (No. 20) to evaluate the crystal structure parameters. The line on the experimental pattern shows the results of these refinements. This is consistent with the experimental results. The values of the crystal structure parameters listed in Table 1 are consistent with those obtained in previous refinements of an X-ray diffraction pattern at room temperature [11].

3.2. McPhase calculations

We evaluated energy levels split by CEFs and magnetic moments using McPhase to investigate the magnetic anisotropy of Tb moments in Tb_3NbO_7 [3, 4, 5]. We calculated CEFs based on the point-charge model using the values of the structural parameters at 12.0 K. We considered all neighboring Tb^{3+}, Nb^{5+}, and O^{2-} ions up to a distance of 20 Å from each Tb^{3+} ion. The numbers of ions are 2532 and 2522 from Tb1 and Tb2 ions, respectively. We obtained the splitting into thirteen ($2J + 1 = 13$) CEF levels (all singlets) owing to the surrounding ions. Here, the magnitude of the total angular momentum, Landé g factor, and magnitude of the moment are $J = 6$, $g_J = 3/2$, and $g_J J = 9\ \mu_B$, respectively, for the ground-state multiplet of Tb^{3+} ions ($4f^8$). The results are presented in Table 2. The ground and first-excited

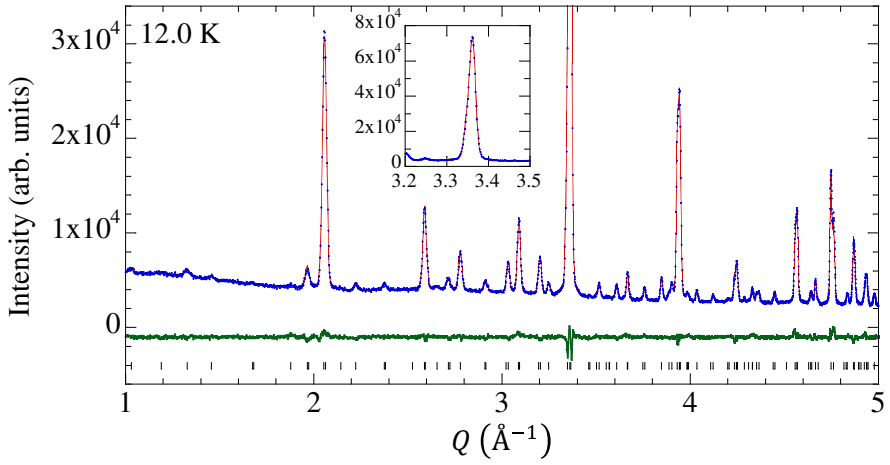

Figure 2: Powder neutron-diffraction pattern (circles) of Tb_3NbO_7 at 12.0 K. The wavelength of the neutrons was 2.450 Å. The line on the measured pattern portrays the Rietveld-refined pattern obtained using the crystal structure with $C222_1$ (No. 20) [11]. The line at the bottom portrays the difference between the measured and Rietveld-refined patterns. The hash marks represent the positions of nuclear reflections. The reliability factors are $\chi^2 = 2.32$, $R_{\rm wp} = 2.97$ %, $R_{\rm exp} = 1.95$ %, and $R_{\rm Bragg} = 3.48$ %. The inset shows the pattern between 3.2 and 3.5 Å^{-1}. The large reflection consists of the three reflections at 0 0 4, 2 4 2, and 4 0 0.

Table 1: Values of crystal-structural parameters of Tb_3NbO_7 derived from the Rietveld refinements of the neutron-diffraction pattern at 12.0 K (upper line of each site). The space group is orthorhombic $C222_1$ (No. 20) [11]. The lattice constants are $a = 7.4660(1)$ Å, $b = 10.5517(2)$ Å, and $c = 7.5023(2)$ Å. The estimated standard deviations are shown in the parentheses. The term $B_{\rm iso}$ denotes the isotropic atomic displacement parameter. The values of $B_{\rm iso}$ of Tb and Nb became negative when they were treated as free parameters. Thus, we set the values to zero. To reduce the number of fitting parameters, we used one value of $B_{\rm iso}$ for O. The reliability factors are $\chi^2 = 2.32$, $R_{\rm wp} = 2.97$ %, $R_{\rm exp} = 1.95$ %, and $R_{\rm Bragg} = 3.48$ %. We also show the values derived from the Rietveld refinements of the X ray diffraction pattern at room temperature (lower line of each site) [11].

Atom	Site	x	y	z	$B_{\rm iso}$ (Å^2)
Tb1	4a	0.4882(5)	0	0	0
		0.4895(7)	0	0	0.36(2)
Tb2	8c	0.2321(2)	0.2346(1)	0.2550(8)	0
		0.2356(3)	0.2346(1)	0.2502(7)	0.36(2)
Nb1	4a	0.9907(6)	0	0	0
		0.9987(9)	0	0	0.03(6)
O1	8c	0.2930(4)	0.3787(4)	0.0215(4)	0.44(2)
		0.295(2)	0.376(2)	0.014(3)	1.1(2)
O2	8c	0.3145(4)	0.3745(3)	0.4637(5)	0.44(2)
		0.309(2)	0.383(2)	0.453(3)	1.1(2)
O3	4b	0	0.6284(3)	0.25	0.44(2)
		0	0.627(2)	0.25	1.1(2)
O4	4b	0	0.3648(3)	0.25	0.44(2)
		0	0.368(2)	0.25	1.1(2)
O5	4b	0	0.0676(3)	0.25	0.44(2)
		0	0.065(2)	0.25	1.1(2)

Table 2: Energy levels (second and fourth columns) of the thirteen states split by CEFs in Tb_3NbO_7 calculated using McPhase based on the point charge model [3, 4, 5]. The third and fifth columns show the energies from the lowest-energy level named 1. The energies of levels 1 and 2 for Tb1 are almost the same but different. Uncertainties due to the experimental errors in the crystal-structural parameters were evaluated using gauss law of error propagation and were shown in parentheses.

	Tb1 ($4a$)	energy (meV)	Tb2 ($8c$)	energy (meV)
13	117.0	233.8(2.6)	115.6	213.6(1.7)
12	117.0	233.8(2.6)	115.6	213.5(1.7)
11	59.5	176.4(2.2)	63.6	161.6(1.3)
10	58.6	175.5(2.2)	63.2	161.1(1.3)
9	22.3	139.2(2.0)	19.1	117.0(1.1)
8	16.3	133.2(1.9)	16.1	114.0(1.0)
7	0.2	117.1(2.0)	-14.0	83.9(1.3)
6	-17.3	99.5(1.6)	-23.6	74.4(0.9)
5	-20.6	96.3(1.6)	-36.8	61.2(1.3)
4	-59.6	57.2(0.8)	-60.2	37.7(0.6)
3	-59.7	57.1(0.8)	-62.8	35.2(0.7)
2	-116.8	0.0(0.0)	-97.8	0.2(0.0)
1	-116.8	0	-98.0	0

states form a quasi doublet that is well separated from the other excited CEF levels.

We calculated magnetic moments at 1 K, where higher CEF levels were not populated, under an external magnetic field of 10 T applied parallel to the three axes. The magnetic moments are presented in Table 3. An external magnetic field induces a magnetic moment that is not oriented parallel to the applied field owing to the CEF anisotropy. The values of $\langle M_c \rangle$ at Tb1 sites are large, indicating that the c axis is the easy axis for Tb1 moments. The anisotropy of Tb2 moments is small. As described later, we used the magnetic anisotropy to select the candidates of IR.

3.3. Magnetic structures at 1.8 and 2.5 K

Figure 3(a) shows the powder neutron diffraction patterns of Tb_3NbO_7 at 1.8 K, 2.5 K (between $T_{N1} = 2.0$ K and $T_{N2} = 3.2$ K), and 12.0 K. At 1.8 K and 2.5 K below T_{N2}, there are numerous reflections that do not exist at 12.0 K. Therefore, they are magnetic reflections. We can index all magnetic reflections using the propagation vector $\mathbf{k}_1 = (0, 0, 0)$ at 1.8 K and

Table 3: Magnetic moments of Tb_3NbO_7 at 1 K in the external magnetic field of 10 T applied parallel to the three axes calculated from the point charge model for the CEFs using McPhase [3, 4, 5]. The values of $\langle M_j \rangle$ $(j = a, b, c)$ are the same at Tb1i and Tb1$(i+2)$ $(i = 1, 2)$ and at Tb2i and Tb2$(i+4)$ $(i = 1 - -4)$. The positions of Tb1$(i+2)$ and Tb2$(i+4)$ are those of Tb1i plus $(\frac{1}{2}, \frac{1}{2}, 0)$ and those of Tb2i plus $(\frac{1}{2}, \frac{1}{2}, 0)$, respectively. Uncertainties due to the experimental errors in the crystal-structural parameters were evaluated using gauss law of error propagation and were shown in parentheses only for Tb11 and Tb21 for simplicity.

$H \parallel a$	position	$\langle M_a \rangle$	$\langle M_b \rangle$	$\langle M_c \rangle$	$\langle M \rangle$
Tb11	$(x, 0, 0)$	0.129(2)	0.000(0)	0.000(0)	0.129(2)
Tb12	$(\bar{x}, 0, \frac{1}{2})$	0.129	0.000	0.000	0.129
Tb21	(x, y, z)	4.801(27)	-6.209(91)	3.863(139)	8.748(168)
Tb22	$(\bar{x}, \bar{y}, z + \frac{1}{2})$	4.801	-6.209	-3.863	8.748
Tb23	$(\bar{x}, y, \bar{z} + \frac{1}{2})$	4.801	6.209	3.863	8.748
Tb24	$(x, \bar{y}, \bar{z})$	4.801	6.209	-3.863	8.748
$H \parallel b$	position	$\langle M_a \rangle$	$\langle M_b \rangle$	$\langle M_c \rangle$	$\langle M \rangle$
Tb11	$(x, 0, 0)$	0.000(0)	1.394(45)	-8.886(8)	8.994(46)
Tb12	$(\bar{x}, 0, \frac{1}{2})$	0.000	1.394	8.886	8.994
Tb21	(x, y, z)	-4.686(27)	6.394(87)	-3.696(140)	8.747(167)
Tb22	$(\bar{x}, \bar{y}, z + \frac{1}{2})$	-4.686	6.394	3.696	8.747
Tb23	$(\bar{x}, y, \bar{z} + \frac{1}{2})$	4.686	6.394	3.696	8.747
Tb24	$(x, \bar{y}, \bar{z})$	4.686	6.394	-3.696	8.747
$H \parallel c$	position	$\langle M_a \rangle$	$\langle M_b \rangle$	$\langle M_c \rangle$	$\langle M \rangle$
Tb11	$(x, 0, 0)$	0.000(0)	-1.234(43)	8.911(6)	8.996(43)
Tb12	$(\bar{x}, 0, \frac{1}{2})$	0.000	1.234	8.911	8.996
Tb21	(x, y, z)	4.720(26)	-6.075(95)	4.180(135)	8.755(167)
Tb22	$(\bar{x}, \bar{y}, z + \frac{1}{2})$	-4.720	6.075	4.180	8.755
Tb23	$(\bar{x}, y, \bar{z} + \frac{1}{2})$	4.720	6.075	4.180	8.755
Tb24	$(x, \bar{y}, \bar{z})$	-4.720	-6.075	4.180	8.755

$\mathbf{k}_2 = (1/2, 1/2, 0)$ at 2.5 K. Figure 3(b) shows the patterns at 1.8 K, 2.2 K, and 2.5 K. We can see magnetic reflections belonging to $\mathbf{k}_1 = (0, 0, 0)$ and those belonging to $\mathbf{k}_2 = (1/2, 1/2, 0)$ at 2.2 K, indicating coexistence of two phases. This result is consistent with the specific heat result (the first-order phase transition at $T_{\mathrm{N1}} = 2.0$ K). Figure 3(c) shows the patterns obtained at various temperatures. Diffuse magnetic scattering is observed at 3.5 K and 5.0 K in the paramagnetic phase.

Symmetric analyses were performed to derive the possible magnetic configurations of 4*a* and 8*c* sites (Tb1 and Tb2 sites, respectively) using programs ISODISTORT [1] and BasIreps [2]. As shown in Table 4, four one-dimensional real IRs are possible for $\mathbf{k}_1 = (0, 0, 0)$ at 1.8 K. Each 4*a* and 8*c* site splits into two independent orbits (without symmetry coupling between them). As shown in Table 5, two IRs are possible for $\mathbf{k}_2 = (1/2, 1/2, 0)$ at the 2.5 K. Each 4*a* and 8*c* site splits into two and four independent orbits, respectively. All Tb1 and Tb2 ions were located at the same crystallographic sites, 4*a* and 8*c* sites, respectively. Therefore, in the refinements, we assumed that magnitudes of components of magnetic moments were the same for all Tb1 (as well Tb2) ions, for example, $|v_{11}| = |v_{12}| = |v_1|$.

Rietveld refinements were performed to determine the magnetic structures. In the refinements, we used the crystal structural parameters determined at 12.0 K. According to the results of the McPhase calculations, the *c* axis is the easy axis for Tb1 moments at 1 K. Therefore, candidates for IR at 1.8 K are $m\Gamma_2$ and $m\Gamma_4$. We found that only $m\Gamma_4$ explains the pattern observed at 1.8 K. At 2.5 K, only $m\mathrm{S}_2$ reproduced the observed pattern. As shown in Table 6, we succeeded in refinements at 2.5 K without Tb1 moments. A Tb22 site has $[u_{21}, v_{21}, \bar{w}_{21}]$, $[u_{21}, v_{21}, \bar{w}_{21}]$, and $[\bar{u}_{21}, \bar{v}_{21}, w_{21}]$ for $m\Gamma_4$, $m\mathrm{S}_2$, and $m\mathrm{S}_1$, respectively, indicating that $m\Gamma_4$ and $m\mathrm{S}_2$ possess the same symmetry. Figure 4 shows the results of the Rietveld refinement at (a) 1.8 K and (b) 2.5 K. The lines on the measured patterns (circles) represent the Rietveld refined patterns including both nuclear and magnetic contributions, and they could reproduce the measured patterns.

Figure 5 shows the magnetic structure. The magnetic moments are presented in Table 6. As expected from the results of the McPhase calculations, the main component of the Tb1 ordered moments is *w* at a 1.8 K. The order of the main components in each chain along the *c* axis is AFM. The small ferromagnetic (FM) *v* components in each chain indicate canting of Tb1 ordered moments. Tb1 moments are disordered at 2.5 K. Tb2 moments form noncollinear magnetic structures in the *ab* plane perpendicular to Tb1 chains

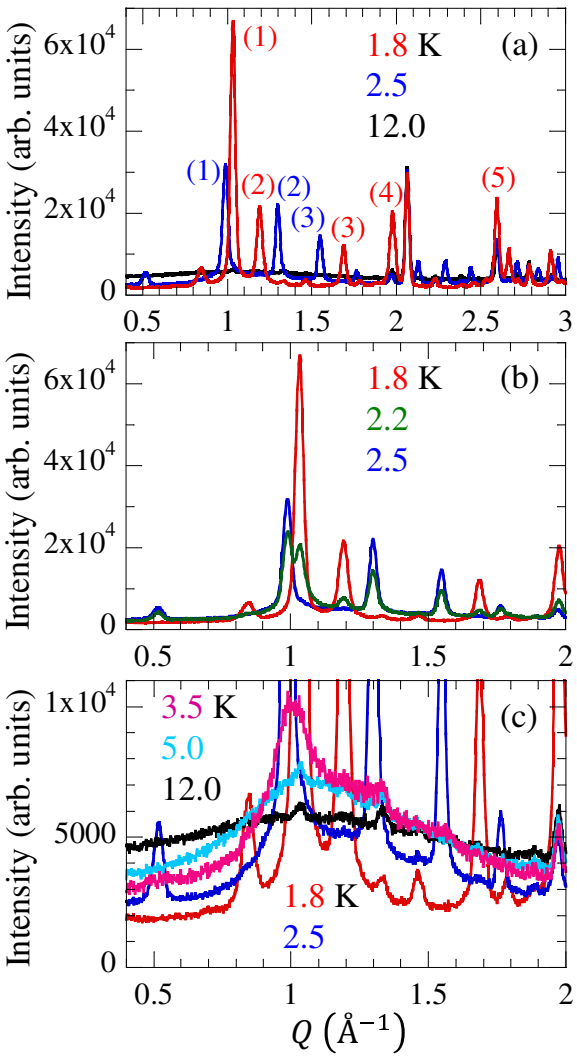

Figure 3: Powder neutron-diffraction patterns of Tb_3NbO_7. The wavelength of the neutrons was 2.450 Å. Indices of the major magnetic reflections are (1) 0 ± 1 1, (2) ± 1 0 1, (3) ± 1 ± 2 1, (4) ± 2 ± 1 1, and (5) ± 2 ± 3 1 for $\mathbf{k}_1 = (0, 0, 0)$ indicated by red numbers. Indices of the major magnetic reflections are (1) ± 0.5 ± 0.5 1, (2) ± 0.5 ± 1.5 1, and (3) ± 1.5 ± 0.5 1 for $\mathbf{k}_2 = (1/2, 1/2, 0)$ indicated by blue numbers.

Table 4: Group theory analysis for the magnetic structure of Tb_3NbO_7 at 1.8 K calculated using the programs ISODISTORT [1] and BasIreps [2]. The crystallographic space group is $C222_1$ (No. 20) [11]. The magnetic propagation vector is $\mathbf{k}_1 = (0, 0, 0)$. The character set corresponds to the following four symmetry elements [2]: Symm(1): 1; Symm(2): 2 $(0, 0, 1/2)$ $0, 0, z$; Symm(3): 2 $0, y, 1/4$; Symm(4): 2 $x, 0, 0$. IR denotes irreducible representation. Tb1 on $4a$ site splits into two independent orbits. Tb2 on $8c$ site splits into two independent orbits. The components of the magnetic moments are expressed using u_{ij}, v_{ij}, and w_{ij} for site i and orbit j.

Character set			(1, 1, 1, 1)	(1, 1, -1, -1)	(1, -1, 1, -1)	(1, -1, -1, 1)
IR (ISODISTORT)			$m\Gamma_1$	$m\Gamma_2$	$m\Gamma_4$	$m\Gamma_3$
IR (BasIreps)			IRrep(1)	IRrep(2)	IRrep(3)	IRrep(4)
Orbit 1	Tb11	$(x, 0, 0)$	$[u_{11}, 0, 0]$	$[0, v_{11}, w_{11}]$	$[0, v_{11}, w_{11}]$	$[u_{11}, 0, 0]$
	Tb12	$(\bar{x}, 0, \frac{1}{2})$	$[\bar{u}_{11}, 0, 0]$	$[0, \bar{v}_{11}, w_{11}]$	$[0, v_{11}, \bar{w}_{11}]$	$[u_{11}, 0, 0]$
Orbit 2	Tb13	$(x + \frac{1}{2}, \frac{1}{2}, 0)$	$[u_{12}, 0, 0]$	$[0, v_{12}, w_{12}]$	$[0, v_{12}, w_{12}]$	$[u_{12}, 0, 0]$
	Tb14	$(\bar{x} - \frac{1}{2}, -\frac{1}{2}, \frac{1}{2})$	$[\bar{u}_{12}, 0, 0]$	$[0, \bar{v}_{12}, w_{12}]$	$[0, v_{12}, \bar{w}_{12}]$	$[u_{12}, 0, 0]$
Orbit 1	Tb21	(x, y, z)	$[u_{21}, v_{21}, w_{21}]$	$[u_{21}, v_{21}, w_{21}]$	$[u_{21}, v_{21}, w_{21}]$	$[u_{21}, v_{21}, w_{21}]$
	Tb22	$(\bar{x}, \bar{y}, z + \frac{1}{2})$	$[\bar{u}_{21}, \bar{v}_{21}, w_{21}]$	$[\bar{u}_{21}, \bar{v}_{21}, w_{21}]$	$[u_{21}, v_{21}, \bar{w}_{21}]$	$[u_{21}, v_{21}, \bar{w}_{21}]$
	Tb23	$(\bar{x}, y, \bar{z} + \frac{1}{2})$	$[\bar{u}_{21}, v_{21}, \bar{w}_{21}]$	$[u_{21}, \bar{v}_{21}, w_{21}]$	$[\bar{u}_{21}, v_{21}, \bar{w}_{21}]$	$[u_{21}, \bar{v}_{21}, w_{21}]$
	Tb24	$(x, \bar{y}, \bar{z})$	$[u_{21}, \bar{v}_{21}, \bar{w}_{21}]$	$[\bar{u}_{21}, v_{21}, w_{21}]$	$[\bar{u}_{21}, v_{21}, w_{21}]$	$[u_{21}, \bar{v}_{21}, \bar{w}_{21}]$
Orbit 2	Tb25	$(x + \frac{1}{2}, y + \frac{1}{2}, z)$	$[u_{22}, v_{22}, w_{22}]$	$[u_{22}, v_{22}, w_{22}]$	$[u_{22}, v_{22}, w_{22}]$	$[u_{22}, v_{22}, w_{22}]$
	Tb26	$(\bar{x} - \frac{1}{2}, \bar{y} - \frac{1}{2}, z + \frac{1}{2})$	$[\bar{u}_{22}, \bar{v}_{22}, w_{22}]$	$[\bar{u}_{22}, \bar{v}_{22}, w_{22}]$	$[u_{22}, v_{22}, \bar{w}_{22}]$	$[u_{22}, v_{22}, \bar{w}_{22}]$
	Tb27	$(\bar{x} - \frac{1}{2}, y + \frac{1}{2}, \bar{z} + \frac{1}{2})$	$[\bar{u}_{22}, v_{22}, \bar{w}_{22}]$	$[u_{22}, \bar{v}_{22}, w_{22}]$	$[\bar{u}_{22}, v_{22}, \bar{w}_{22}]$	$[u_{22}, \bar{v}_{22}, w_{22}]$
	Tb28	$(x + \frac{1}{2}, \bar{y} - \frac{1}{2}, \bar{z})$	$[u_{22}, \bar{v}_{22}, \bar{w}_{22}]$	$[\bar{u}_{22}, v_{22}, w_{22}]$	$[\bar{u}_{22}, v_{22}, w_{22}]$	$[u_{22}, \bar{v}_{22}, \bar{w}_{22}]$

Table 5: Group theory analysis for the magnetic structure of Tb_3NbO_7 at 2.5 K calculated using the programs ISODISTORT [1] and BasIreps [2]. The crystallographic space group is $C222_1$ (No. 20) [11]. The magnetic propagation vector is $\mathbf{k}_2 = (1/2, 1/2, 0)$. The character set corresponds to the following two symmetry elements [2]: Symm(1): 1; Symm(2): 2 $(0, 0, 1/2)$ $0, 0, z$. IR denotes irreducible representation. Tb1 on $4a$ site splits into two independent orbits. Tb2 on $8c$ site splits into four independent orbits. The components of the magnetic moments are expressed using u_{ij}, v_{ij}, and w_{ij} for site i and orbit j.

Character set			(1, 1)	(1, -1)
IR (ISODISTORT)			$m\mathrm{S}_1$	$m\mathrm{S}_2$
IR (BasIreps)			IRrep(1)	IRrep(2)
Orbit 1	Tb11	$(x, 0, 0)$	$[u_{11}, v_{11}, w_{11}]$	$[u_{11}, v_{11}, w_{11}]$
	Tb12	$(\bar{x}, 0, \frac{1}{2})$	$[\bar{u}_{11}, \bar{v}_{11}, w_{11}]$	$[u_{11}, v_{11}, \bar{w}_{11}]$
Orbit 2	Tb13	$(x + \frac{1}{2}, \frac{1}{2}, 0)$	$[u_{12}, v_{12}, w_{12}]$	$[u_{12}, v_{12}, w_{12}]$
	Tb14	$(\bar{x} - \frac{1}{2}, -\frac{1}{2}, \frac{1}{2})$	$[\bar{u}_{12}, \bar{v}_{12}, w_{12}]$	$[u_{12}, v_{12}, \bar{w}_{12}]$
Orbit 1	Tb21	(x, y, z)	$[u_{21}, v_{21}, w_{21}]$	$[u_{21}, v_{21}, w_{21}]$
	Tb22	$(\bar{x}, \bar{y}, z + \frac{1}{2})$	$[\bar{u}_{21}, \bar{v}_{21}, w_{21}]$	$[u_{21}, v_{21}, \bar{w}_{21}]$
Orbit 2	Tb23	$(\bar{x}, y, \bar{z} + \frac{1}{2})$	$[u_{22}, v_{22}, w_{22}]$	$[u_{22}, v_{22}, w_{22}]$
	Tb24	$(x, \bar{y}, \bar{z})$	$[\bar{u}_{22}, \bar{v}_{22}, w_{22}]$	$[u_{22}, v_{22}, \bar{w}_{22}]$
Orbit 3	Tb25	$(x + \frac{1}{2}, y + \frac{1}{2}, z)$	$[u_{23}, v_{23}, w_{23}]$	$[u_{23}, v_{23}, w_{23}]$
	Tb26	$(\bar{x} - \frac{1}{2}, \bar{y} - \frac{1}{2}, z + \frac{1}{2})$	$[\bar{u}_{23}, \bar{v}_{23}, w_{23}]$	$[u_{23}, v_{23}, \bar{w}_{23}]$
Orbit 4	Tb27	$(\bar{x} - \frac{1}{2}, y + \frac{1}{2}, \bar{z} + \frac{1}{2})$	$[u_{24}, v_{24}, w_{24}]$	$[u_{24}, v_{24}, w_{24}]$
	Tb28	$(x + \frac{1}{2}, \bar{y} - \frac{1}{2}, \bar{z})$	$[\bar{u}_{24}, \bar{v}_{24}, w_{24}]$	$[u_{24}, v_{24}, \bar{w}_{24}]$

Table 6: Magnetic moments of Tb_3NbO_7. All Tb1 and Tb2 ions were located at the same crystallographic sites, $4a$ and $8c$ sites, respectively. Therefore, we assumed that magnitudes of components of magnetic moments were the same for all Tb1 (as well Tb2) ions, for example, $|v_{11}| = |v_{12}| = |v_1|$. Parameters m_1 and m_2 denote the magnitude of the magnetic moments of Tb1 and Tb2.

Temperature	1.8 K	2.5 K
Propagation vector	$\mathbf{k}_1 = (0, 0, 0)$	$\mathbf{k}_2 = (1/2, 1/2, 0)$
IR	$m\Gamma_4$	$m\mathrm{S}_2$
Tb11 $(0.488, 0, 0)$	$[0, v_1, w_1]$	
Tb12 $(-0.488, 0, 0.5)$	$[0, v_1, \bar{w}_1]$	
Tb13 $(0.988, 0.5, 0)$	$[0, \bar{v}_1, \bar{w}_1]$	
Tb14 $(-0.988, -0.5, 0.5)$	$[0, \bar{v}_1, w_1]$	
Tb21 $(0.232, 0.235, 0.255)$	$[u_2, v_2, w_2]$	$[u_2, v_2, w_2]$
Tb22 $(-0.232, -0.235, 0.755)$	$[u_2, v_2, \bar{w}_2]$	$[u_2, v_2, \bar{w}_2]$
Tb23 $(-0.232, 0.235, 0.245)$	$[\bar{u}_2, v_2, \bar{w}_2]$	$[\bar{u}_2, v_2, \bar{w}_2]$
Tb24 $(0.232, -0.235, -0.255)$	$[\bar{u}_2, v_2, w_2]$	$[\bar{u}_2, v_2, w_2]$
Tb25 $(0.732, 0.735, 0.255)$	$[\bar{u}_2, \bar{v}_2, \bar{w}_2]$	$[\bar{u}_2, \bar{v}_2, \bar{w}_2]$
Tb26 $(-0.732, -0.735, 0.755)$	$[\bar{u}_2, \bar{v}_2, w_2]$	$[\bar{u}_2, \bar{v}_2, w_2]$
Tb27 $(-0.732, 0.735, 0.245)$	$[u_2, \bar{v}_2, w_2]$	$[u_2, \bar{v}_2, w_2]$
Tb28 $(0.732, -0.735, -0.255)$	$[u_2, \bar{v}_2, \bar{w}_2]$	$[u_2, \bar{v}_2, \bar{w}_2]$
v_1 (μ_B)	-1.16(5)	
w_1 (μ_B)	7.22(10)	
m_1 (μ_B)	7.31(10)	
u_2 (μ_B)	-3.66(6)	3.64(8)
v_2 (μ_B)	6.48(4)	5.31(6)
w_2 (μ_B)	1.57(3)	-1.76(4)
m_2 (μ_B)	7.60(6)	6.68(3)

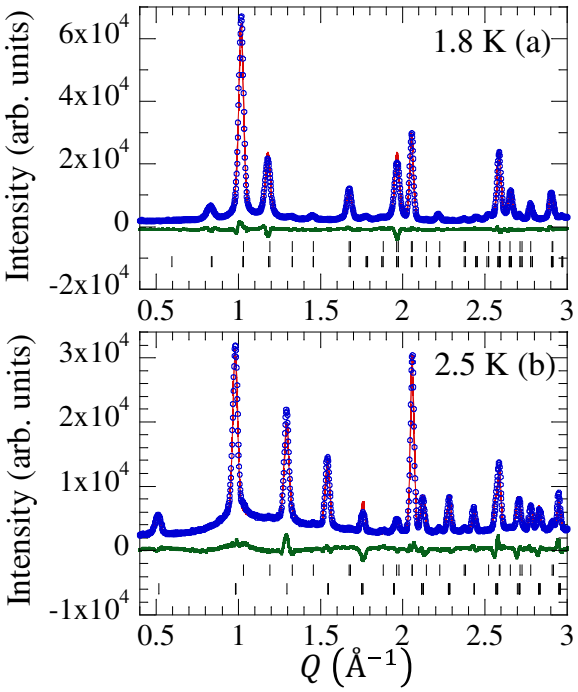

Figure 4: Powder neutron-diffraction pattern (circles) of Tb_3NbO_7. The wavelength of the neutrons was 2.450 Å. The magnetic propagation vector and IR are $\mathbf{k}_1 = (0, 0, 0)$ and $m\Gamma_4$ at 1.8 K (a) and $\mathbf{k}_2 = (1/2, 1/2, 0)$ and $m\mathrm{S}_2$ at 2.5 K (b). The line on the measured pattern portrays the Rietveld-refined pattern including both nuclear and magnetic contributions. We used atomic parameters determined by Rietveld refinements for the pattern at 12.0 K using orthorhombic $C222_1$ (No. 20). The line at the bottom portrays the difference between the measured and Rietveld-refined patterns. The upper and lower hash marks represent the positions of the nuclear and magnetic reflections, respectively. The reliability factors are $\chi^2 = 6.81$ and 12.1, $R_{\mathrm{wp}} = 5.01$ and 6.75 %, $R_{\mathrm{exp}} = 1.92$ and 1.94 %, $R_{\mathrm{Bragg}} = 2.02$ and 3.55 %, and $R_{\mathrm{mag}} = 3.04$ and 7.22 % at 1.8 (a) and 2.5 K (b), respectively.

with a small w component at both the 1.8 K and 2.5 K. The magnetic structure at 1.8 K is consistent with the magnetic anisotropies obtained using the McPhase calculations. Only Tb2 moments are ordered at 2.5 K, indicating the appearance of the partially disordered state observed in several frustrated antiferromagnets [12, 24, 26, 29, 22, 23, 28, 25, 27, 30]. The magnitudes of the Tb1 and Tb2 moments at 1.8 K are smaller than the theoretical values ($g_J J = 9\ \mu_B$) probably because of frustration among exchange interactions. Our results are consistent with the following results reported in [11]. The first and second order phase transitions occur at $T_{N1} = 2.0$ and $T_{N2} = 3.2$ K, respectively. Tb1 and Tb2 moments are ordered at $T_{N1} = 2.0$ and $T_{N2} = 3.2$ K, respectively. No spontaneous magnetization appears. Both the broad maximum at around 4 K in the magnetic susceptibility and the diffuse magnetic scattering at around 3.5 K and 5.0 K indicate existence of short-range magnetic correlations.

3.4. Comparison of magnetic structures of Tb_3RuO_7 and Tb_3NbO_7

Magnetic structures of Tb moments in Tb_3RuO_7 at 1.5 K [Fig. 1(a)] [12] and Tb_3NbO_7 at 1.8 K (Fig. 5) were found to be similar. This similarity indicates that the influence of Ru moments on the magnetic structure of Tb moments is weak except for the high transition temperature ($T_N = 17$ K) because of the Tb-Ru exchange interactions in Tb_3RuO_7. The T dependences of the magnitude of Tb1 moments were also found to be similar. In Tb_3RuO_7, the magnitude is large [8.58(2) μ_B] and small [1.78(12) μ_B] at 1.5 and 15 K, respectively. In Tb_3NbO_7, the magnitude is large [7.97(8) μ_B] and zero at 1.8 and 2.5 K, respectively ($T_{N2} = 3.2$ K). Here, we refer to Tbi with $i = 1 - 2$ (Tb1) and Tbi with $i = 3 - 6$ (Tb2) moments for Tb_3RuO_7 (Tb_3NbO_7) as the chain and plane moments, respectively. The easy axis of the chain moments is parallel to the chains, whereas the plane moments are mainly ordered perpendicular to the chains. Therefore, the exchange interactions between the chain and plane moments force chain moments to be perpendicular to the chains, indicating that competition between anisotropy and exchange interactions occurs. Consequently, we propose the following hypothesis: chain moments cannot develop at 15 K and 2.5 K in Tb_3RuO_7 and Tb_3NbO_7, respectively.

We considered the reasons why two transitions and one transition appear in Tb_3NbO_7 and Tb_3RuO_7, respectively. In Tb_3NbO_7, the order of the Tb1 moments is the origin of transition at T_{N1}. In addition, the propagation vector was changed from $\mathbf{k}_2 = (1/2, 1/2, 0)$ to $\mathbf{k}_1 = (0, 0, 0)$. Chain and

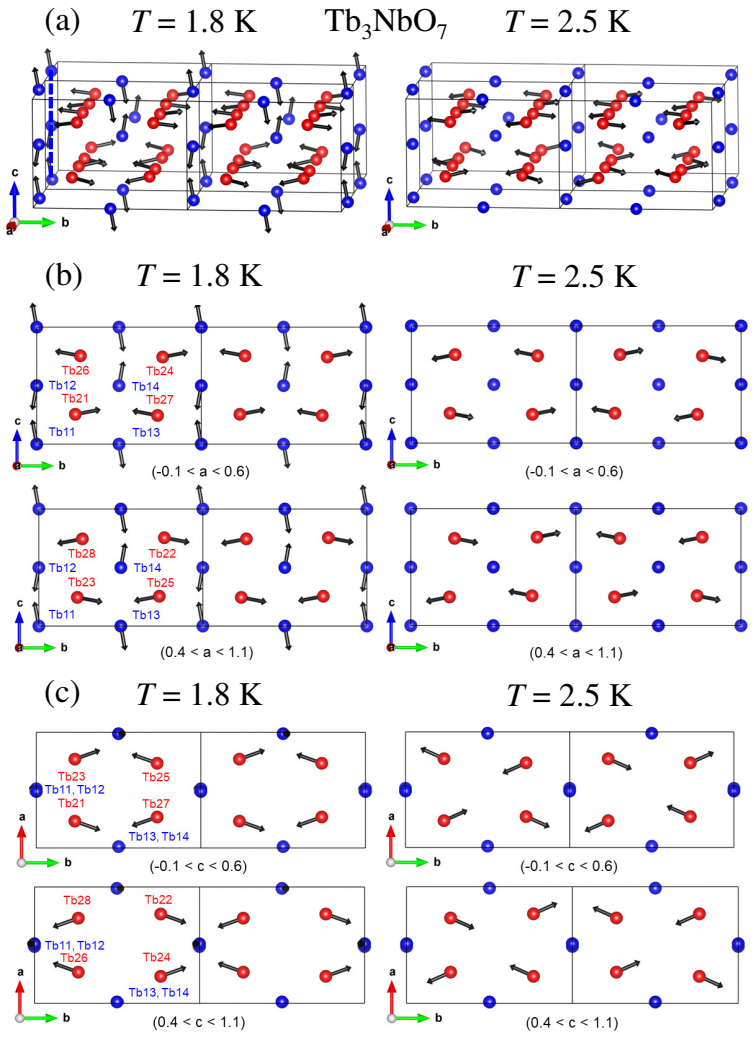

Figure 5: Magnetic structures of Tb_3NbO_7 shown as three dimensional (a) and as projections onto the *bc* (b) and *ab* planes (c) drawn using VESTA [18]. The magnetic propagation vector and IR are $\mathbf{k}_1 = (0, 0, 0)$ and $m\Gamma_4$, respectively, at 1.8 K and $\mathbf{k}_2 = (1/2, 1/2, 0)$ and mS_2, respectively, at 2.5 K. The blue and red circles denote Tb1 and Tb2 sites, respectively. The vertical dashed line in (a) indicates a Tb1 chain.

plane moments prefer the FM and AFM arrangements, respectively, in the a and b directions. We speculate that the transition from $\mathbf{k}_2 = (1/2, 1/2, 0)$ to $\mathbf{k}_1 = (0, 0, 0)$ occurs because chain moments become dominant in the arrangement of moments below T_{N1}. In Tb_3RuO_7, all Tb moments prefer the FM arrangements along the a and c directions (chains $\parallel$ b) and no further transition occurs.

4. Summary

We determined the magnetic structures of Tb_3NbO_7 based on powder neutron diffraction experiments and magnetic anisotropy calculations. We calculated the energy levels split by CEFs and the magnetic moments using McPhase. The c axis is the easy axis for Tb1 moments, and magnetic anisotropy is small for Tb2 moments. Magnetic reflections were observed at low temperatures. The propagation vector is $\mathbf{k}_1 = (0, 0, 0)$ at 1.8 K and $\mathbf{k}_2 = (1/2, 1/2, 0)$ at 2.5 K between transition temperatures $T_{\mathrm{N1}} = 2.0$ K and $T_{\mathrm{N2}} = 3.2$ K. Magnetic anisotropy was used to select candidates for IRs of the magnetic structures. We determined that the IRs are $m\Gamma_4$ and mS_2 at 1.8 K and 2.5 K, respectively, from Rietveld refinements. The main component of Tb1 ordered moments (chain moments) is w at 1.8 K. The order of the main components in each chain along the c axis is AFM. Small FM v components in each chain indicate the canting of Tb1 ordered moments. Tb1 moments are disordered at 2.5 K. Tb2 moments (plane moments) form noncollinear magnetic structures in the ab plane perpendicular to Tb1 chains with a small w component at both the 1.8 K and 2.5 K. The magnetic structure at 1.8 K is consistent with the the magnetic anisotropies obtained using McPhase calculations. Only Tb2 moments are ordered at 2.5 K, indicating the appearance of the partially disordered state observed in several frustrated antiferromagnets. Magnetic structures of Tb moments in Tb_3RuO_7 at 1.5 K and Tb_3NbO_7 at 1.8 K are similar, indicating that the influence of Ru moments on magnetic structure of Tb moments is weak. We speculate that competition between magnetic anisotropy and exchange interactions between chain and plane moments generates the small and zero chain moments in Tb_3RuO_7 at 15 K and Tb_3NbO_7 at 2.5 K, respectively. We also speculate that the transition from $\mathbf{k}_2 = (1/2, 1/2, 0)$ to $\mathbf{k}_1 = (0, 0, 0)$ at T_{N1} in Tb_3NbO_7 occurs because the chain moments become dominant for the arrangement of moments below T_{N1}.

Acknowledgments

This study was supported by Japan Society for the Promotion of Science (JSPS) KAKENHI Grant No. 18K03551. JST-Mirai Program Grant No. JPMJMI18A3, Japan, and the World Premier International Research Center Initiative (WPI), Ministry of Education, Culture, Sports, Science and Technology (MEXT), Japan. This study is partially based on the experiments performed on the HRPT diffractometer (Proposal No. 20212393) at the Swiss Spallation Neutron Source SINQ, the Paul Scherrer Institute, Switzerland. We thank Seiko Matsumoto at the National Institute for Materials Science (NIMS) for the sample synthesis and X-ray diffraction measurements. We also thank Masamichi Nishino, Kazunari Yamaura Alexei Belik, and Yoshihiro Tsujimoto at NIMS for their insightful discussions.

References

[1] B. J. Campbell, H. T. Stokes, D. E. Tanner, and D. M. Hatch, ISODISPLACE: An internet tool for exploring structural distortions, J. Appl. Cryst. 39 (2006) 607; [https://stokes.byu.edu/iso/isodistort.php].

[2] J. Rodriguez-Carvajal, Recent advances in magnetic structure determination by neutron powder diffraction, Physica B 192 (1993) 55; [http://www.ill.eu/sites/fullprof/].

[3] M. Rotter, Using McPhase to calculate magnetic phase diagrams of rare earth compounds, J. Magn. Magn. Mater. 272 (2004) e481.

[4] M. Rotter, M. D. Le, A. T. Boothroyd, and J. A. Blanco, Dynamical matrix diagonalization for the calculation of dispersive excitations, J. Phys.: Condens. Matter 24 (2012) 213201.

[5] T. Stöter, M. Doerr, and M. Rotter, A new theoretical approach to the strain dependence of magnetic crystal-field anisotropy, Eur. Phys. J. B 94 (2021) 125.

[6] M. Rotter, A. Schneidewind, M. Doerr, M. Loewenhaupt, A.M. El Massalami, and C. Detlefs, Interpreting magnetic X-ray scattering on Gd-compounds using the McPhase simulation program, Physica B 345 (2004) 231.

[7] M. Rotter and A. T. Boothroyd, Going beyond the dipole approximation to improve the refinement of magnetic structures by neutron diffraction, Phys. Rev. B 79 (2009) 140405(R).

[8] M. Rotter, M. D. Le, H. Lewtas, A. T. Boothroyd, J.A. Blanco, and R. Hammerling, Calculation of Atomic Charge- Moment- and Current densities using McPhase, a versatile modeling suite for Magnetic Neutron Scattering, J. Phys. Conf. Series 325 (2011) 012005.

[9] M. Loewenhaupt, P. Geselbracht, E. Faulhaber, M. Rotter, M. Doerr, K. Schmalzl, and A. Schneidewind, Field dependence of the magnetic propagation vector of the heavy fermion compound $CeCu_2Ge_2$ studied by neutron diffraction, Phys Procedia 75 (2015) 230.

[10] M. Rotter and M. Doerr, McPhase model calculations of the magnetic phase diagram of $CeCu_2Ge_2$ - Prediction of a double q magnetic structure, Comp. Mater. Sci. 142 (2018) 206.

[11] Y. Doi, Y. Harada, and Y. Hinatsu, Crystal structures and magnetic properties of fluorite-related oxides Ln_3NbO_7 (Ln = lanthanides), J. Solid State Chem. 182 (2009) 709.

[12] M. Hase, A. Dönni, and V. Yu. Pomjakushin, Magnetic structures of nearly isostructural Tb_3RuO_7 and Nd_3RuO_7: Appearance of a partially disordered state only in the Tb compound, Phys. Rev. B 104 (2021) 214430.

[13] M. Hase, A. Dönni, V. Yu. Pomjakushin, K. Nawa, D. Okuyama, T. J. Sato, S. Asai, and T. Masuda, Magnetic excitations of the spin-chain compound Tb_3RuO_7, JPS Conf. Proc. 38 (2023) 011129.

[14] Y. Hinatsu and Y. Doi, Structural phase transition and antiferromagnetic transition of Tb_3RuO_7, J. Solid State Chem. 220 (2014) 22.

[15] W. A. Groen, F. P. F. van Berkel, and D. J. W. IJdo, Trineodymium ruthenate(V). A Rietveld refinement of neutron powder diffraction data, Acta Crystallogr. C 43 (1987) 2262.

[16] D. Harada, Y. Hinatsu, and Y. Ishii, Studies on the magnetic and structural phase transitions of Nd_3RuO_7, J. Phys.: Condens. Matter 13 (2001) 10825.

[17] M. Wakeshima and Y. Hinatsu, Magnetic properties and structural transitions of orthorhombic fluorite-related compounds Ln_3MO_7 (Ln = rare earths, M = transition metals), J. Solid State Chem. 183 (2010) 2681.

[18] K. Momma and F. Izumi, VESTA for three-dimensional visualization of crystal, volumetric and morphology data, J. Appl. Cryst. 44 (2011) 1272.

[19] A. N. Klimenko, V. M. Ionov, N. A. Tomilin, V. S. Sergeev, V. P. Sirotinkin, A. E. Prozorovskii, V. B. Rybakov, and S. G. Zhukov, Phase transitions in the lanthanide niobates R_3NbO_7 at high temperatures, Russ. J. Inorg. Chem. 35 (1990) 338; Zh. Neorg. Khim. 35 (1990) 599.

[20] A. N. Klimenko, Y. S. Kozlov, V. S. Sergeev, and E. A. Pastukhov, High temperature phase transitions in rare-earth element niobates R_3NbO_7, Thermochim. Acta 209 (1992) 331.

[21] P. Fischer, G. Frey, M. Koch, M. Koennecke, V. Pomjakushin, J. Schefer, R. Thut, N. Schlumpf, R. Buerge, U. Greuter, S. Bondt, and E. Berruyer, High-resolution powder diffractometer HRPT for thermal neutrons at SINQ, Physica B 276-278 (2000) 146; [http://sinq.web.psi.ch/hrpt].

[22] M. Mekata, Antiferro-ferrimagnetic transition in triangular Ising lattice, J. Phys. Soc. Jpn. 42 (1977) 76.

[23] M. Mekata, N. Yaguchi, T. Takagi, T. Sugino, S. Mitsuda, H. Yoshizawa, N. Hosoito, and T. Shinjo, Successive magnetic ordering in $CuFeO_2$ -A new type of partially disordered phase in a triangular lattice antiferromagnet, J. Phys. Soc. Jpn. 62 (1993) 4474.

[24] S. Vilminot, M. Richard-Plouet, G. André, D. Swierczynski, M. Guillot, F. Bourée-Vigneron, and M. Drillon, Magnetic structure and properties of $Cu_3(OH)_4SO_4$ made of triple chains of spins $s = \frac{1}{2}$, J. Solid State Chem. 170 (2003) 255.

[25] J. R. Stewart, G. Ehlers, A. S. Wills, S. T. Bramwell, and J. S. Gardner, Phase transitions, partial disorder and multi-k structures in $Gd_2Ti_2O_7$, J. Phys.: Condens. Matter 16 (2004) L321.

[26] S. Vilminot, G. André, F. Bourée-Vigneron, M. Richard-Plouet, and M. Kurmoo, Magnetic properties and magnetic structures of $Cu_3(OH)_4XO_4$, X = Se or S: Cycloidal versus collinear antiferromagnetic structure, Inorg. Chem. 46 (2007) 10079.

[27] M. Matsuda, J.-H. Chung, S. Park, T. J. Sato, K. Matsuno, H. Aruga Katori, H. Takagi, K. Kakurai, K. Kamazawa, Y. Tsunoda, I. Kagomiya, C. L. Henley, and S.-H. Lee, Frustrated minority spins in $GeNi_2O_4$, Europhys. Lett. 82 (2008) 37006.

[28] M. Matsuda, C. de la Cruz, H. Yoshida, M. Isobe, R. S. Fishman, Partially disordered state and spin-lattice coupling in an $S = \frac{3}{2}$ triangular lattice antiferromagnet Ag_2CrO_2, Phys. Rev B 85 (2012) 144407.

[29] M. Hase, H. Kuroe, V. Yu. Pomjakushin, L. Keller, R. Tamura, and N. Terada Y. Matsushita, A. Dönni, and T. Sekine, Magnetic structure of the spin-$\frac{1}{2}$ frustrated quasi-one-dimensional antiferromagnet $Cu_3Mo_2O_9$: Appearance of a partially disordered state, Phys. Rev B 92 (2015) 054425.

[30] M. Hase, A. Dönni, N. Terada, V. Yu. Pomjakushin, J. R. Hester, K. C. Rule, and Y. Matsuo, Neutron diffraction studies under zero and finite magnetic fields of the $\frac{1}{2}$ quantum magnetization plateau compound $Ni_2V_2O_7$, Phys. Rev B 107 (2023) 224415.